

Spatially Localized Chemical Patterns around an $A + B \rightarrow$ Oscillator Front

M. A. Budroni,^{*,†,§} L. Lemaigre,^{‡,§} D. M. Escala,[¶] A. P. Muñuzuri,[¶] and A. De Wit[‡]

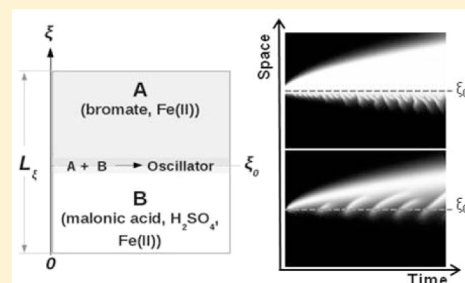
[†]Department of Chemistry and Pharmacy, University of Sassari, 07100 Sassari, Italy

[‡]Université libre de Bruxelles (ULB), Nonlinear Physical Chemistry Unit, Faculté des Sciences, CP231, 1050 Brussels, Belgium

[¶]Nonlinear Physics Group, University of Santiago de Compostela, 15782 Santiago de Compostela, Spain

Supporting Information

ABSTRACT: When two gels, each loaded with a different set of reactants A and B of an oscillatory reaction, are brought into contact, reaction–diffusion patterns such as waves or Turing patterns can develop in the reactive contact zone. The initial condition which separates the reactants at the beginning leads to a localization in space of the different dynamical regimes accessible to the chemical oscillator. We study here both numerically and experimentally the composite traveling structures resulting from the interaction between chemical fronts and localized waves in the case in which the reactants of such an $A + B \rightarrow$ oscillator system are those of the canonical Belousov–Zhabotinsky (BZ) oscillating reaction. A transition between different dynamics is obtained by varying the initial concentration of the organic substrate of the BZ reactants, which is one of the parameters controlling the local excitability. We show that the dynamical regime (excitable or oscillatory) characterizing the BZ oscillator in the initial contact area is the key feature which determines the spatiotemporal evolution of the system. The experimental results are in qualitative agreement with the theoretical predictions.



INTRODUCTION

Reaction fronts are encountered in a wide range of biological, physical, and chemical systems. Some of these fronts develop when two reactants, A and B, initially separated in space diffuse one toward the other and react along the simple chemical reaction $A + B \rightarrow C$. Since the pioneering work of Gálfi and Rácz,¹ numerous theoretical^{2,3} and experimental^{4–6} works have been devoted to characterizing the properties of the related $A + B \rightarrow C$ reaction–diffusion (RD) fronts. Such fronts provide the basis for understanding examples of localized patterns such as Liesegang bands⁷ (and related applications in material science⁸) and of more complex systems in which different mechanisms come into play cooperatively as in chemical gardens⁹ (and related applied problems^{10,11}).

In the absence of a gel, chemical fronts may be perturbed by convective flows. The dynamics resulting from the coupling of an $A + B \rightarrow C$ chemical reaction with diffusion and hydrodynamic flows have been studied in both vertically^{12,13} and horizontally oriented reactors.¹⁴ The related reaction–diffusion–convection (RDC) problem is at the heart of many applications ranging from extraction^{15,16} to CO₂ sequestration^{17,18} techniques. Depending on the relative contribution of each chemical species to the local density or viscosity of the solutions, the evolution and morphology of the chemical front can dramatically change. In turn, the chemical reaction can impact and modify the topology of the hydrodynamic instabilities as compared to the nonreactive case.¹⁹ In this framework, knowing the dynamical properties of the RD concentration profiles controlling the hydrodynamics con-

stitutes the essential building block to predict the symmetries of the associated RDC patterns.

A current challenge in RDC pattern formation around reactive interfaces is to go beyond the simple $A + B \rightarrow C$ case and include more complex kinetics, such as autocatalytic or oscillatory mechanisms. The objective is to understand to what extent the self-organizing properties of the chemical system can feed back on the hydrodynamic pattern and vice versa. When coupled to diffusion, nonlinear reactions are known to give rise to a wealth of spatiotemporal patterns.^{20,21,43} Traditionally these RD patterns are investigated in gels used to avoid convection, in which the reactants are initially homogeneously distributed. In these conditions, autocatalytic fronts separating the reacted from the nonreacted solution can propagate through the chemical medium if a clock reaction is at play,²² while traveling waves²³ or Turing patterns⁴⁰ can develop if the chemical kinetics is ruled by an oscillatory mechanism. There is an extensive literature in which the properties of these RD structures have been analyzed both theoretically and experimentally.²⁰ In the absence of gels, such chemical traveling structures can also trigger hydrodynamic motions²⁵ due to local gradients of density^{26–28} and/or surface tension^{29–31} across the front creating buoyancy- and/or Marangoni-driven flows. The onset of convective motions can not only distort the shape and enhance the velocity of a traveling front but also induce new

Received: November 4, 2015

Revised: January 2, 2016

Published: January 4, 2016

chemo-hydrodynamic patterns³² and bifurcations in the system dynamics,³³ including the transition to chemical chaos.^{34–36} More recently, RDC patterns have been studied around oscillating dynamics obtained when two solutions containing separate reactants of the oscillating Belousov–Zhabotinsky (BZ) reaction are put in contact along a horizontal line in the gravity field.³⁷ The complexity of the coupling between convective and chemical dynamics calls for an understanding of the underlying RD patterns at the origin of density gradients triggering the flows.

In this context, the objective here is to investigate the RD dynamics developing when a chemical oscillator is spatially bridled between two separated pools of initial reactants slowly diffusing one into the other (see Figure 1). This specific

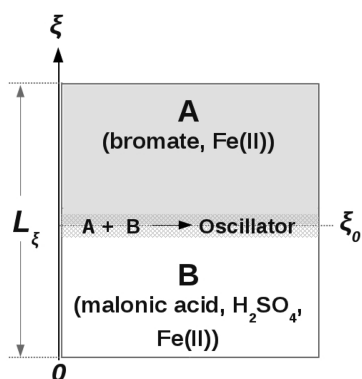


Figure 1. Sketch of the double-layer system $A + B \rightarrow$ oscillator.

configuration allows the localization of the nucleation and development of the RD dynamics in the interfacial reactive zone between the two reactant pools. In gels, Turing patterns localized in space because of feeding of the gel from the sides have already been studied in previous theoretical and experimental works.^{38–43} Experiments with gels fed laterally on each border with different reactant solutions have also been performed in an annular reactor by using the BZ system.^{44–46} Sustained wavetrains (so-called “excyclons”) have been seen to develop in the azimuthal direction in the central mixing zone of the gel where reactants meet by diffusion and react. The spatial confinement of this oscillating zone could be the source of a localized periodic chemical forcing of hydrodynamic motions in the case of similar experiments performed without gels.³⁷ Here we provide a classification of the possible RD scenarios where interfacial localized waves and chemical fronts can emerge. The problem is studied by means of a combined numerical and experimental approach, considering the prototype BZ oscillating reaction. Two gels separately containing isolated main reactants of the BZ system are put in contact, and the BZ reaction can take place across the mixing interface between these regions. As the initial reactants diffuse toward each other, the system develops in space different dynamical regimes (typically oscillatory or excitable) of the BZ oscillator. As a result, autocatalytic fronts can coexist and interact with trigger waves. This interplay between traveling structures has already been shown to cause breaks of spatiotemporal symmetry such as the transition from target to spiral waves in homogeneous media.⁴⁷ Differently from other studies where the spatial extent of the local regions with different excitability and dynamical regimes is induced externally (for instance by means of illumination of a photosensitive BZ medium⁴⁸), here this is

controlled in situ through the initial concentration of the main reactants, their diffusivity, and the kinetic parameters of the chemical process. We first give a numerical exploration and a characterization of how these factors influence the global dynamics. A parametric study is carried out by using a mathematical model based on the Field, Körös, and Noyes (FKN) mechanism⁴⁹ (Numerical Study). Experimental scenarios are presented in Experimental Study and interpreted in light of the theoretical results. Conclusions are drawn in Concluding Discussion.

NUMERICAL STUDY

Modeling. Kinetics. The BZ mixture is an acidic solution containing bromate ions and an oxidable organic substrate which, in the presence of a suitable one-electron redox catalyst (typically cerium(IV) salts or ferroin), can give rise to oscillations in the concentration of some of the reaction intermediates. The complex kinetic mechanism underlying the 0-dimensional behavior (i.e., in a well-stirred mixture) has been described by Field, Körös, and Noyes.⁴⁹ They provided a detailed set of reactions able to reproduce the shape of the oscillations and the response of the dynamical behavior to given parameters, such as the initial concentration of the main reactants and the temperature. The FKN mechanism can be reduced to a minimal set of kinetic steps which constitutes the skeleton of the Oregonator model.²² As discussed in the Supporting Information, the Oregonator consists of a preparatory oxidation phase (OP) where an autocatalytic species forms and drives the system from the reduced to the oxidized state ($\text{Fe(II)} \rightarrow \text{Fe(III)}$ (blue), if ferroin is used as catalyst). A second phase (the so-called “resetting of the chemical clock”) is an oversimplification of the process by which the reactive mixture is turned back to the reduced state ($\text{Fe(III)} \rightarrow \text{Fe(II)}$) through the oxidation of the organic substrate (typically malonic acid or 1,4-cyclohexanedione).

In the dimensionless form, the kinetic equations describing the OP read

$$\frac{dx}{d\tau} = \frac{1}{\epsilon_1} [-hxy + qah^2y - x^2 + (1 - z/z_m)/(1 - z/z_m + \epsilon)ahx] \quad (1)$$

$$\frac{dy}{d\tau} = -\frac{1}{q}hxy - ah^2y \quad (2)$$

$$\frac{dz}{d\tau} = (1 - z/z_m)/(1 - z/z_m + \epsilon)ahx \quad (3)$$

where the variables a , h , x , y , and z are the dimensionless concentrations of the bromate, sulfuric acid, autocatalytic intermediate HBrO_2 , inhibitor Br^- , and oxidized form of the catalyst, respectively. $\{q, \epsilon, \epsilon_1, z_m\}$ is the set of kinetic parameters which depend on the rate constants and the dimensional concentration of the initial reactants (A_0 , bromate; H_0 , sulfuric acid) as detailed in the Supporting Information.

The dimensionless model which governs the bulk behavior of the full BZ system including the resetting step is

$$\frac{dx}{d\tau} = \frac{1}{\epsilon_1} [-hxy + qah^2y - x^2 + (1 - z/z_m)/(1 - z/z_m + \epsilon)ahx] \quad (4)$$

$$\frac{dy}{d\tau} = \frac{1}{\epsilon_2} (-hxy - qah^2y + bz) \quad (5)$$

$$\frac{dz}{d\tau} = (1 - z/z_m)/(1 - z/z_m + \epsilon)ahx - bz \quad (6)$$

where b is the dimensionless concentration of the organic substrate.

In this complete Oregonator model (eqs 4–6) and in the OP model (eqs 1–3), we implicitly consider the dimensionless equations $\dot{d}a = \dot{d}b = \dot{d}h = 0$ for the main reactants which dimensional concentration corresponds to $A = A_0a$, $B = B_0b$, and $H = H_0h$. This means that we neglect the depletion of reactants as they are slowly consumed as compared to the time scale characterizing the RD dynamics of the intermediate species.²² This assumption is particularly reliable for the BZ reaction which is able to stay in quasi-stationary conditions in the far-from-equilibrium branch long enough to allow sustained dissipative dynamics such as oscillations to be maintained quite a long time in batch reactors before going back to equilibrium. We generally indicate kinetic functions with $F_i([j]$ th species, \mathbf{k}), where $j = i = \{a, b, h, x, y, z\}$ and \mathbf{k} is the set of the kinetic parameters $\{\epsilon, \epsilon_1, \epsilon_2, q, z_m\}$.

Spatially Extended System. By coupling the kinetic functions to Fickian diffusion, we get the dimensionless RD equations

$$\partial_t[i] - \delta_i \partial_\zeta^2[i] = F_i([j], \mathbf{k}) \quad \forall \text{ } i\text{th concentration field} \quad (7)$$

where δ_i is the ratio of the diffusivity of the i th species to the reference $D \sim 1.5 \times 10^{-5} \text{ cm}^2 \text{ s}^{-1}$. In the aqueous phase, the diffusion coefficients of all BZ species are around this value²² except for the protons whose diffusivity is around 4 times greater. The dimensional diffusivity reference, D , is used to define our spatial scale, $r_0 = \sqrt{Dt_0}$, and thus the dimensionless space coordinate, $\zeta = r/r_0$, where r represents the corresponding dimensional spatial variable.

The equation set 7 describes the dynamics and patterns in spatially distributed systems due to the interplay between the BZ nonlinear kinetics and diffusive transport. Reaction–diffusion patterns have been typically studied with the Oregonator model by considering the initial BZ reactants homogeneously distributed over the reactor and their constant concentration values are then included in the kinetic parameters. When the BZ medium is oscillatory, phase-diffusion waves form and dominate the system dynamics (see ref 47 and references therein) while solitary pulses or stable wave trains occur in excitable conditions (see ref 50 and references therein). The kinetic parameters can modify the properties of these traveling structures. In particular, ϵ_1 and ϵ_2 govern the excitability of the system and thus the relaxation of the wave after the excitation. When the system is oscillatory, the effect of an increase in q on traveling waves is to decrease the wave period and the excursion amplitude of phase-diffusion waves. Depending upon the values of the initial concentration of the reactants (and hence of ϵ_1 and ϵ_2) the variation of q can also bring the system to the excitable regime and solitary pulses or wave trains may form if a single or a periodic perturbation are applied to the medium, respectively.

As compared to the classic formulation of the Oregonator model, we explicitly introduce the main reactants (a, b, h) as variables of the RD system 7. In practice, we solve eqs 1–3 or 4–6 with diffusion terms coupled to pure diffusion equations for the reactants (a, b, h) as their reactive consumption is neglected. We initially impose step function distributions for these reactant species (see details in the following section). Their local concentration thus changes in space and time

through diffusion, inducing a change of local stability conditions and chemical dynamics in the course of time.

Initial Conditions and Numerical Approach. The system 7 is solved by using the Crank–Nicolson method over a one-dimensional spatial domain (a vertical cut of the double-layer stratification sketched in Figure 2a) of dimensionless length L_ζ

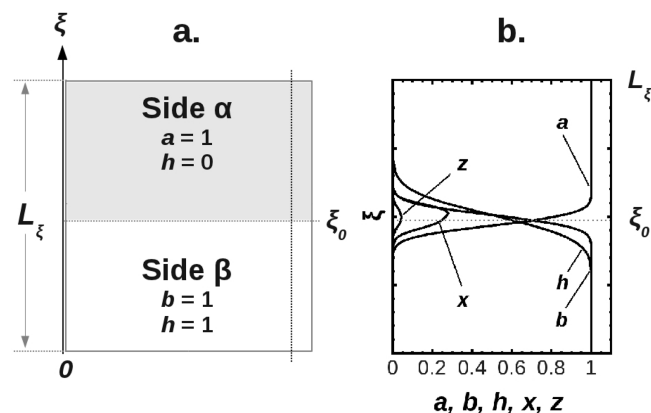


Figure 2. (a) Sketch of the initial distribution of the reactants (compare with Table 1). The dotted line perpendicular to the initial interface between the two layers represents the one-dimensional spatial domain over which simulations are performed. (b) Typical spatial profiles of the chemical concentrations (a, b, h, x, z) during the first instants of the dynamics.

= 100, discretized on a grid of 200 points (i.e., spatial mesh $h_\zeta = 0.5$). No-flux boundary conditions are imposed on the concentration fields at the boundaries of the reactor. Simulations are run for 50 time units, using the integration time step $h_\tau = 1 \times 10^{-4}$, which was tested to avoid convergence problems due to the stiffness of the differential equations (4–6). All the diffusivity ratios δ_i are set to 1, except for $\delta_h = 4$ as the protons are known to diffuse faster than the other species.

As stressed in the Introduction and in the previous section, the key aspect of our problem is the initial separate distribution of the main reactants, such that the BZ reaction can start only once the reactants start to diffuse one into the other. The oscillating dynamics remains then localized around the interface between the two pools of reactants. The interfacial localization of the oscillator can be obtained with several initial conditions of the reactant concentrations in which at least one of the species $\{a, b, h\}$ is separated from the others. However, in the following we consider only one reference configuration introduced in the study of RD excyclons⁴⁶ and which is currently used in ongoing investigations on chemo-hydrodynamic problems in double-layer systems. The step functions describing this initial distribution of the reactants are detailed in Table 1.

Conventionally, we will refer in the text to side α as the reactor domain $\zeta \geq \zeta_0$ where at $\tau = 0$ $a(\zeta, 0) = 1$ while the notation side β will identify the region $\zeta \leq \zeta_0$ where $b(\zeta, 0) = 1$. The spatiotemporal profiles of the reactant concentration follow the analytical form $b(\zeta, \tau) = \frac{1}{2} \operatorname{erfc}\left(\frac{\zeta - \zeta_0}{2\sqrt{\delta_b \tau}}\right)$, $h(\zeta, \tau) = \frac{1}{2} \operatorname{erfc}\left(\frac{\zeta - \zeta_0}{2\sqrt{\delta_h \tau}}\right)$, and $a(\zeta, \tau) = \frac{1}{2} \operatorname{erfc}\left(\frac{-\zeta + \zeta_0}{2\sqrt{\delta_a \tau}}\right)$ where ζ_0 is the initial contact point between the two reactant pools (see Figure 2b). With respect to the widely explored cases in which the BZ

Table 1. Step Functions Describing the Initial Spatial Profiles of the Reactant Concentrations

reactant	initial concentration
$a(\zeta, 0)$	1 if $\zeta \geq \zeta_0$ 0 elsewhere
$b(\zeta, 0)$	1 if $\zeta \leq \zeta_0$ 0 elsewhere
$h(\zeta, 0)$	1 if $\zeta \leq \zeta_0$ 0 elsewhere

reactants are assumed as constant and homogeneously distributed over the spatial domain, this double-layer configuration confers a nonstationary nature to our problem because the reactant distribution depends upon space and time and a , b and h feature, de facto, true variables of the system. (This nomenclature should not be confused with contexts in which the term stationary refers to static and stable chemical patterns such as those triggered by a Turing instability). x , y , $z = 0$ over the whole spatial domain (except for a seed of z at the reactor interface). The concentration scales of the sulfuric acid, the bromate salt and the ferroin are $H_0 = 0.2$ M, $A_0 = 0.3$ M, $C_0 = 0.005$ M, respectively.

In this double-layer system, the reaction is localized across the mixing area of the main reactants where the intermediates form (see Figure 2b).

We explore the spectrum of possible dynamics as a function of the excitability parameter which is traditionally defined as the ratio $(A_0 \times H_0)/B_0$. While in the pool approximation conditions this is a constant, embedded in the parameter ϵ_1 for the two-variable classic Oregonator, here the excitability and the dynamical regime depend upon space and time as tuned by the spatially varying concentrations $a(\zeta, \tau)$, $b(\zeta, \tau)$ and $h(\zeta, \tau)$. Nevertheless, varying B_0 allows us to change the initial dynamical regime of the system at ζ_0 and hence to set the local excitability in this region. The nature of the initial regime across the interface is a crucial feature which determines the spatiotemporal morphology of resulting chemical patterns and is used hereafter as a reference to classify the system. Numerical simulations are carried out with $q = 0.01$ which enables us to induce changes in the dynamics (from oscillatory to excitable conditions) by varying the initial concentration of the reactants (see Supporting Information).

Results. Autocatalytic Kinetics. We first consider the case of the simple oxidation front in the absence of the organic substrate ($b = 0 \forall \zeta$) and no oscillations can thus be obtained.

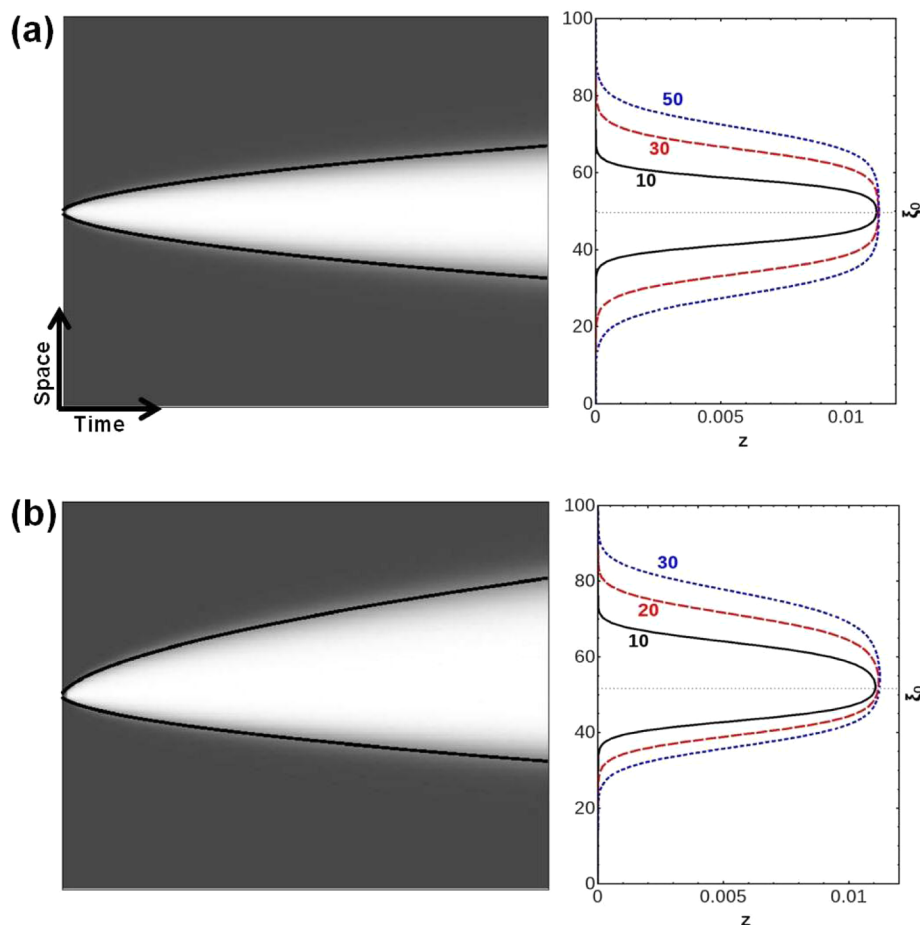


Figure 3. Spatiotemporal evolution (100 space units \times 50 time units) of the concentration z when only the autocatalytic process OP (i.e., $b = 0$) is operative across the initial interface ζ_0 . Panel a shows on the left the space–time plots of the oxidized front (bright area) and, on the right, the concentration profiles of species z at 10 (black solid line), 20 (red dashed line), and 50 (blue dotted line) time units, when $\delta_h = 1$; panel (b) plots the same for $\delta_h = 4$; the black solid line, red dashed line, and blue dotted line describe the z concentration profiles at 10, 20, and 30 time units, respectively. In both simulations the starting ratio $H_0/A_0 = 0.6$. The black curves over the space–time plots describe the trends obtained from eqs 8 and 9.

This preliminary case is instructive to gradually extend the characterization of the RD structures from the classic $A + B \rightarrow C$ case¹ to an autocatalytic mechanism (here reading $A + H \rightarrow$ autocatalysis).

The sulfuric acid (h) diffuses from side β into side α containing bromate (a) (and vice versa), and the autocatalytic oxidation described in the OP model can only take place ($b = 0$) at the interface. Starting from the interfacial area, the reduced form ($z = 0$) of the catalyst, homogeneously spread over the whole spatial coordinate, is progressively transformed into the oxidized form ($z \neq 0$), allowing us to follow the oxidation dynamics (see Figure 3).

To better understand the properties of this autocatalytic chemical front, let us first recall those of the classic $A + B \rightarrow C$ RD problem. It has been shown analytically^{1–3} that for $A + B \rightarrow C$ fronts the front position (i.e., the point along the spatial coordinate where the production rate is maximum) travels as a square root of time, toward a direction which depends on (i) the ratio of initial reactant concentrations and (ii) the diffusion coefficients. As can be inferred from the space–time plots shown in Figure 3, similar features also characterize the oxidized front in the autocatalytic case under analysis. In Figure 3 we compare the spatiotemporal dynamics of the reaction front obeying the OP reactive scheme when species a and h have the same diffusivity (panel a) or when the ratio $\delta_h = D_H/D_A$ equals 4 (panel b). The global phenomenology of the two systems is similar: as soon as the two main reactants meet, an autocatalytic front of the oxidized catalyst z nucleates at the center of the reactor and grows through both opposite layers following a diffusion-limited process. The spatial concentration profile of species z shows a characteristic sigmoidal shape as illustrated in the right panels of Figure 3. In both cases the initial concentration ratio H_0/A_0 equals 0.6, but in contrast to the $A + B \rightarrow C$ case, the dynamics is unaffected by the relative concentration of the two reactants. We can appreciate in Figure 3a how the oxidation front develops symmetrically toward both sides while its growth is asymmetric in the case of a different diffusivity of the two reactants (Figure 3b). The dominant diffusivity between the two chemical species actually determines the preferential growth direction of the front.

By contrast with a homogeneous initial condition (i.e., in which A and H are initially homogeneously distributed in the reactor), here the front speed is not isotropic and constant but is correlated to the local concentration of $a(\zeta, \tau)$ and $h(\zeta, \tau)$. When H diffuses faster into A , it triggers the front propagation along the same direction and, in turn, drives its asymmetric development.

In order to give a more quantitative description of the front dynamics, we recall that if the autocatalytic front propagates in a homogeneous medium, its dimensional speed is given by $c = \sqrt{4k_4DA_0H_0}$. In our problem, we can redefine a local front velocity as $c(\zeta, \tau) = \sqrt{4k_4DA_0a(\zeta, \tau)H_0h(\zeta, \tau)}$, which, scaled by our reference velocity $c_0 = \sqrt{k_2DA_0H_0^2}$, reads

$$\bar{c} = \sqrt{\frac{k_4}{k_2H_0} \operatorname{erfc}\left(\frac{-(\zeta - \zeta_0)}{2\sqrt{\tau}}\right) \operatorname{erfc}\left(\frac{(\zeta - \zeta_0)}{2\sqrt{\delta_h\tau}}\right)} \quad (8)$$

where $k_2 = 2 \text{ s}^{-1} \text{ M}^{-3}$ and $k_4 = 42 \text{ s}^{-1} \text{ M}^{-2}$ are the rate constants characterizing the formation of the intermediate HBrO_2 and its autocatalysis, respectively (see Supporting Information). Starting from the reactor center, where the front is initiated,

we can follow the evolution of the front tips (ζ_{tip}^+ , moving toward $\zeta > \zeta_0$; ζ_{tip}^- , moving toward $\zeta < \zeta_0$) by numerically iterating the formula

$$\zeta_{\text{tip}}^{\pm}(\tau) = \zeta_{\text{tip}}^{\pm}(\tau - h_{\tau}) \pm \bar{c}h_{\tau} \quad (9)$$

The evolution of the front computed by means of eqs 8 and 9, shown as black curves in Figure 3, is in good agreement with the spatiotemporal behaviors obtained from the numerical simulations.

Oscillatory or Excitable BZ Kinetics. We next explore the interfacial dynamics around the contact line of the two-layer system for the initial condition shown in Figure 2a, i.e., for the complete BZ kinetics. The concentration of the organic substrate B_0 is varied in the range [0.06, 0.6] M. The left panels of Figure 4 describe the change in the system dynamics when it switches from the excitable to the oscillatory regime at the contact area (see the definition in Modeling), by plotting the space–time map of the concentration of z for four different values of B_0 . Space–time plots are built by piling as a function

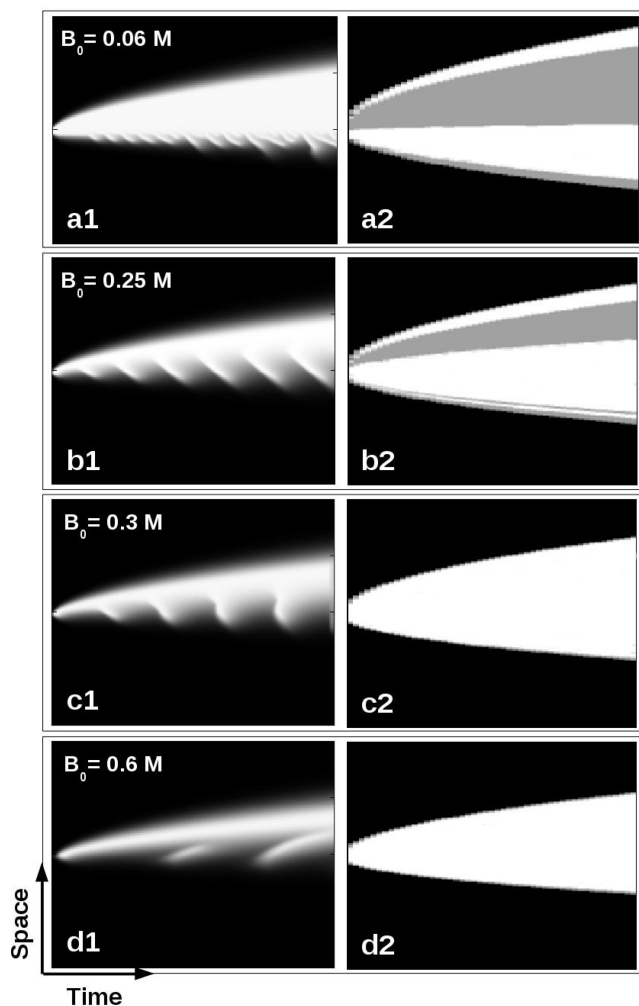


Figure 4. Overview of the dynamical scenarios obtained for different values of B_0 . For each B_0 value, the panels show, on the left, the space–time plots (100 space units \times 50 time units) of the catalyst concentration and, on the right, the corresponding evolution of the local dynamical regimes of the chemical oscillator along the spatial coordinate (black, nonreactive; gray, excitable; and white, oscillatory).

of time (horizontal axis) the one-dimensional spatial profile of the catalyst concentration (vertical axis).

As a general feature, we can observe how the fast diffusing acid immediately triggers in zone α an oxidation front led by the species x and z . These intermediates form at the contact line and propagate preferentially toward layer α , while their concentration declines to zero in side β . After an induction period (IP), waves appear and coexist with the oxidation front. To interpret this phenomenology, we compare the concentration space–time plots to the dynamical regimes accessible to the chemical system over the spatial coordinate (right panels of Figure 4), i.e., the corresponding 0-dimensional dynamics obtained by integrating the kinetics (eqs 4–6) with the local values of a , b , and h at every 0.1 time units. Black areas identify the regions where no reaction takes place, as the concentration of at least one of the main reactants is too low; gray and white areas identify the excitable and oscillatory regimes, respectively.

When the initial concentration B_0 is in the range [0.06, 0.30] M, the excitable regime dominates the dynamics across the interface, inducing an initial delay for the onset of the trigger waves (see Figure 4, panels a1–b2). This delay corresponds to the time needed to create a critical spatial region where the system is locally oscillatory, whose extent is compatible with the minimal wavelength required for a stable wavetrain.⁴⁷ Oscillatory conditions are met just below ζ_0 , where A is fed from the layer α by diffusive transport and the concentration of both the acid and the organic substrate are the highest within the reactor. The area where waves can develop extends in time mainly toward side β because in the opposite layer the concentration of B is too low and the system stabilizes to the oxidized state. It is important to notice that waves emanate from the main oxidation front and travel in the same direction as A diffuses. The line which separates the oxidized region from waves (i.e., the border dividing the spatial regions where the system is excitable and oscillatory, respectively) remains almost constant during the simulation. In the course of time the shape of the waves in the spatiotemporal description slowly changes and becomes more complex for two main reasons: (i) As discussed in the previous section, the temporal dependence of the local concentration of a and h , which constitute the substrate for the development of the oxidized waves, affects the local velocity of the wave. Typically, we register a decrease of the local velocity below ζ_0 in zone β (in fact, here the bright stripes describing the wave dynamics show a decreasing slope) because the maximum velocity value (i.e., where $a(\zeta, \tau) \times h(\zeta, \tau)$ is maximum) presents a drifting in time toward side α , as $\delta_i > 1$. This factor has to be combined with (ii) the interaction between new waves and refractory areas left by previous traveling structures, which inhibit the development of new waves. Recall that refractory areas are subsets of the spatial domain, rich in bromide ions, where the BZ medium has not recovered yet from a previous excitation and thus cannot undergo a new excitation or support oxidation wave propagation. Both effects (i) and (ii) are at the basis of complex space–time patterns showing waves that increase and decrease intermittently in the extent toward side β .

The dynamics drastically change when the concentration of B_0 is increased (Figure 4, panels c1–d2). An oxidation front still develops toward side α ; however, the width of the oxidized state zone decreases and, in turn, the wave domain pervades side α too. Interestingly, when $B_0 \geq 0.30$ M and the system switches from the initial excitable to the oscillatory regime, the morphology of the wave is reversed in space and time with

respect to the case $B_0 \leq 0.30$ M (compare Figure 4, panels b1 and b2 and Figure 4, panels d1 and d2). In the last case, waves nucleate at the middle of the reactor and follow (eventually annihilate with) the leading oxidation front. This behavior is reminiscent of stacking waves observed by Steinbock and co-workers in the 1,4-cyclohexanedione BZ (CHD-BZ) system.⁵⁰ The dynamics at the threshold value $B_0 = 0.30$ M, in which the spatiotemporal dynamics of the waves changes symmetry, is framed in the space–time map Figure 4, panel c1. There can be observed the coexistence of waves starting in parallel from the oxidation front and from the initial interface, resulting in an S-shaped space–time pattern.

The changes in the spatiotemporal dynamics of the system when it switches from the excitable to the oscillatory regime is also characterized in Figure 5, where we analyze the length of

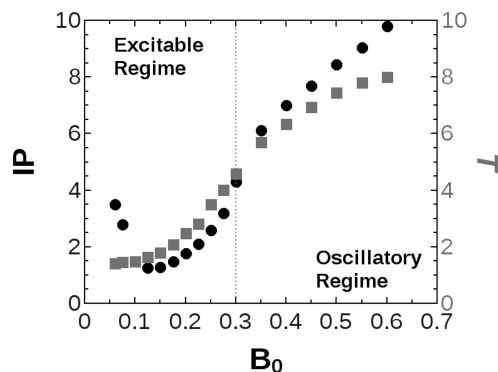


Figure 5. Induction period (IP, black circles) needed for the onset of the localized traveling waves and characteristic period of the waves (T , gray squares) as a function of B_0 .

the induction period needed for the onset of the waves and their characteristic period (T) as a function of B_0 . T was measured from the time–space plots like in Figure 4 as the distance between successive peaks along the temporal coordinate at the initial contact point, ζ_0 . To compute the characteristic period of the waves we considered the first oscillations as T presents a smooth increment in time because of the nonstationary nature of the system. The dependence of T on B_0 , shown with gray squares, describes a monotonically increasing trend which is consistent with the parallel decrement of the local excitability of the system. The behavior of $IP(B_0)$ (black circles) is correlated with T , though the former exhibits a more complicated shape. At low values of B_0 , there is an increase of IP due, as mentioned above, to the fact that the system is dominantly in its oxidized state and it takes time to develop an area where the oscillatory instability and waves set in. For B_0 values larger than 0.1 M, the IP is mainly determined by the system's characteristic oscillation period across the interfacial area; hence, $IP(B_0)$ closely follows $T(B_0)$. It is worth noting that at $B_0 \sim 0.30$ M, where the break of symmetry in the spatiotemporal behavior of the waves occurs, both the curves $IP(B_0)$ and $T(B_0)$ change concavity.

EXPERIMENTAL STUDY

Dynamical patterns around a spatially localized oscillator were investigated experimentally by separating the BZ reactants in two different gels put in contact along a line in order to initiate the reaction at the interface. Experiments were also performed in a one-dimensional configuration (i.e., in a capillary) to ensure the compatibility with the one-dimensional simulations

presented above. However, after checking the consistency between the dynamics obtained with the one-dimensional and a two-dimensional configuration (i.e., in a Petri dish), the parametric study was carried out in a two-dimensional configuration which makes the experimental procedure and the data analysis easier.

Experimental Setup. Two different gels were prepared by mixing aqueous stock solutions of the BZ reactants with a solution of agarose at a temperature above the gelling point to obtain a final concentration of 0.40% agarose (Sigma, for molecular biology). These liquid mixtures were poured into a Petri dish on either side of a narrow spacer separating the spatial domain into two equal sectors where the mixtures gelled. The final thickness of the gel was of 1 mm. One gel (α) contains only bromate and ferroin while the other one (β) is a mixture of malonic acid (MA), sulfuric acid, and ferroin. The spacer was then removed and the gels pushed one against the other to initiate the propagation of species through the whole spatial domain and the chemical reaction across the contact area. Finally, the Petri dish was covered with its glass lid and the residual volume inside the reactor filled with nitrogen to avoid contact of the gels with oxygen. A schematic view of the Petri dish setup seen from above is sketched in Figure 6.

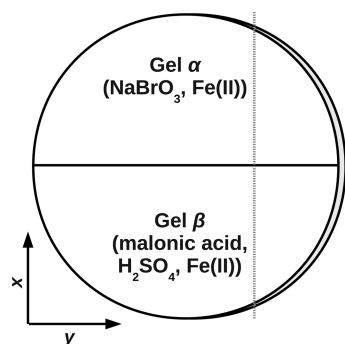


Figure 6. Sketch of the 2D experimental setup. The dotted line perpendicular to the contact line between the two gels represents the one-dimensional section used to build up the space–time plots.

All reactants were commercial grade and used without any further purification. The stock solutions of the main reactants were prepared with distilled water and NaBrO_3 (Sigma, puriss. p.a.), H_2SO_4 (Fluka, volumetric solution), and malonic acid (Merck). Ferroin was prepared by mixing $\text{FeSO}_4 \cdot 7\text{H}_2\text{O}$ (VWR, reagent grade) and 1,10-phenanthroline (Fluka, puriss. p.a.) in a molar ratio 1:3. Working solutions were obtained by additive volumes of the stock solutions to obtain the final concentrations presented in Table 2.

Gels were prepared in the same way to study the dynamics in a one-dimensional geometry. Instead of being poured into a

Table 2. Concentrations of the Reactants in the Two Gels^a

Reactant	Concentration in gel α (mol/L)	Concentration in gel β (mol/L)
ferroin	0.00100	0.00100
NaBrO_3	[0.100, 0.300]	0
malonic acid	0	[0, 0.800]
H_2SO_4	0	0.200

^aThe concentrations of NaBrO_3 and malonic acid are varied for the parametric exploration of the system.

Petri dish, the solutions above their gelling point were injected from both sides into a capillary tube (inner diameter, 1 mm) with an exhaust at midlength to allow the two fluids to come in contact. The results (not shown here) are consistent with those obtained in two dimensions and confirm that the comparison between one-dimensional simulations and two-dimensional experiments is reliable.

Both one- and two-dimensional experiments were recorded with a digital camera at a speed of one frame every 10 s for 6 h by using a lightpad as a light source to better resolve the contrast between oxidized and reduced areas. As water condensation gradually accumulated on the lid during the experiment and hindered the visualization from the top, the camera was put under the Petri dish and hence the lightpad was above it. The images were processed and analyzed by means of Matlab and the free software ImageJ. All the experiments were carried out at room temperature.

Spatiotemporal Dynamics. As in the Numerical Study, we explore chemical RD patterns developing at the interface between the two gels by analyzing the morphology of the related spatiotemporal plots when either the concentration of the malonic acid or of bromate is varied (Figure 7). These plots

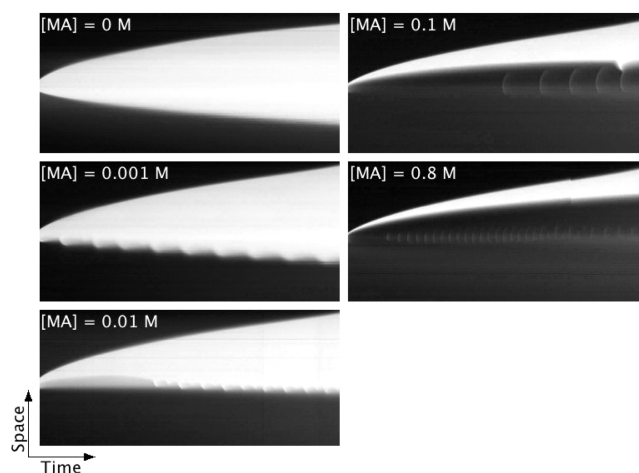


Figure 7. Experimental space–time plots of the catalyst dynamics at different initial concentrations of the malonic acid ($[\text{NaBrO}_3] = 0.300 \text{ M}$). Side α is shown on top. The real dimension of each plot is 5 cm \times 250 min.

are drawn from a line perpendicular to the initial interface. The vertical and the horizontal axes represent space and time, respectively. Bright areas correspond to the regions where the catalyst is in the oxidized form (Fe(III) , ferroin) while dark areas identify reduced regions (Fe(II) , ferroin). As shown in Table 2, in our experiments the concentration of malonic acid ranges from the limit case 0 to 0.800 M.

Autocatalytic Front. When there is no malonic acid in side β , an oxidized front propagates after contact of both gels toward both sides α and β , because no waves can develop in the absence of an organic substrate. Consistent with what was explained in the Numerical Study and Figure 3, the first space–time plot in Figure 7 features a planar front which grows asymmetrically because of the higher diffusivity of the protons with respect to the other species. The propagation speed of this autocatalytic front is not constant in time because the initial reactant distribution is not homogeneous and their concentrations vary both in space and time. In Figure 8, panels a and b

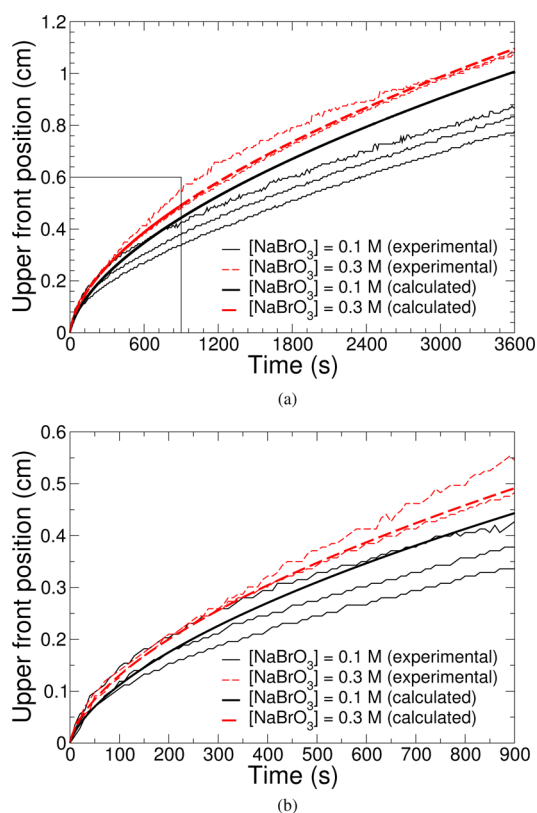


Figure 8. (a) Propagation of the oxidation front toward side α . Experimental curves for $[\text{NaBrO}_3] = 0.100$ M (black solid lines) and 0.300 M (red dashed lines) are compared to the profiles calculated numerically via the dimensional form of eqs 8 and 9 with the same concentration values of bromate, $H_0 = 0.2$ M, $D = 1.4 \times 10^{-5}$, and $k_4 = 42 \text{ s}^{-1} \text{ M}^{-2}$. Panel b is a magnification of the frame in panel a describing the first 900 s where both experimental dynamics show a good agreement with the calculated trend.

illustrate the comparison between the evolution of the upper front position obtained experimentally and numerically thanks to the dimensional form of eqs 8 and 9 for two different initial concentrations of NaBrO_3 . We compare the experimental trends performed with $[\text{NaBrO}_3] = 0.100$ M (black solid lines) and 0.300 M (red dashed lines) to the corresponding calculated profiles. In general, the numerical and the experimental curves follow the same qualitative behavior. The agreement between them is better for the higher concentration of bromate. This is probably due to the fact that the temporal depletion of NaBrO_3 and H_2SO_4 by the chemical reaction is neglected in eqs 8 and 9, and this assumption better fits the system for high concentrations of the initial reactants which keep it in quasi-stationary regimes for longer periods. Vice versa for low starting concentrations, the dimensional eq 8 gives an overestimation of this interpretation is the convergence of the numerical and experimental curves during the first stages of the dynamics that can be better appreciated.

Wave Dynamics. The spatiotemporal dynamics becomes more complex if the initial concentration of malonic acid is increased. As a general feature (see Figure 7) we can observe the coexistence of the oxidized front invading side α with waves which appear later in time and develop through side β .

For low concentration values of malonic acid, the waves start from the leading oxidized front and travel toward side β ($[\text{MA}]$

$= 0.0010$ and 0.0100 M in Figure 7). On the other hand, if the initial concentration of the organic substrate is increased, not only do waves nucleate at the front but also additional waves emerge around the contact line between the gels and move toward both sides of the gel ($[\text{MA}] = 0.100$ and 0.800 M in Figure 7).

By comparing the space–time plots of Figures 4 and 7, we can appreciate how the experimental findings are consistent with the scenarios predicted from the numerical analysis.

Following the characterization drawn for the numerical simulations, we measure the induction period and the characteristic period of the waves. Because the experiments are carried out in a closed system, the waves are transient and the wave period changes during time. As a consequence, the wave period is measured only during the 30 min following the occurrence of the first wave. However, for some experiments the first period already exceeds 30 min, in which case this first period is measured and included in the results shown in Figure 9. The parallel between Figures 5 and 9 shows that the

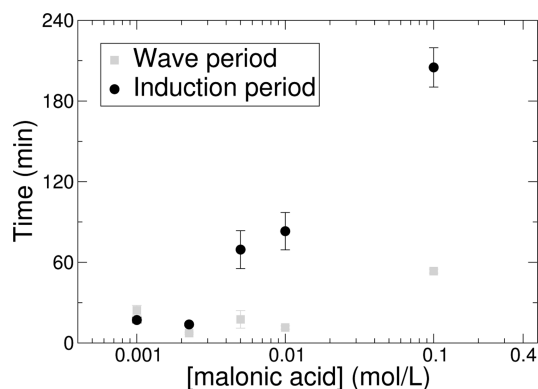


Figure 9. Characterization of the experimental dynamics by means of the mean induction period for the onset of the waves (black circles) and the related wave period (gray squares) as a function of $[\text{MA}]$ ($[\text{NaBrO}_3] = 0.3$ M). The values are averaged over two experiments.

induction period (black circles) and the wave period (gray squares) describe qualitative trends similar to those obtained from the numerical analysis. Indeed, the induction period also increases with increasing $[\text{MA}]$. However, in the experiments we cannot span the malonic acid concentration to high values ($[\text{MA}] \geq 0.400$ M) as both the induction and wave periods become too long.

In general, we observe that the induction period is markedly greater than the wave period, indicating that the diffusion-limited characteristic time to create a suitable region for the onset of waves is greater than the characteristic time of reaction–diffusion dynamics.

The spatiotemporal dynamics observed experimentally are very similar to those found numerically. They feature not only the same qualitative characteristics but also analogous trends when the initial concentrations of the reactants are varied. Surprisingly, the more favorable comparison between simulations and experiments is obtained when the parameter q of the Oregonator model is 0.01 instead of the 0.00015 ± 5 value expected for the BZ system.

CONCLUDING DISCUSSION

In a spatially extended system, the localization of RD dynamics around the contact line between two solutions containing

separately the main initial reactants of an oscillatory reaction can induce the coexistence of oscillatory and excitable regimes over the spatial domain and, in turn, the interaction between localized chemical fronts and waves. We have here first given a classification of these scenarios by means of a RD model, where the Oregonator kinetic scheme is coupled to Fickian diffusion with an initial condition on concentrations such that the reactants are initially separated in two subparts of the system. Upon contact and diffusion of the reactants one into the other, an oxidation front or oscillatory and excitable waves can be obtained starting from the zone of contact between the solutions. Depending upon the initial concentration of the organic substrate, we can change the spatial distribution of the dynamical regimes accessible to the oscillator and control the development of different spatiotemporal patterns. For low values of the organic substrate, typically in the [0.02–0.30] M range, an oxidized front propagates toward the side containing the bromate (side α), and from this oxidized area waves emanate toward the side containing the organic substrate (side β). For larger concentrations of the organic species, the system switches to spatiotemporal evolutions in which the waves nucleate at the interface and follow the leading oxidized front in side α while they travel as solitary pulses in the layer β in the spatial domain where the system is oscillatory. The characterization of this transition reveals that the change in the morphology of the spatiotemporal plots corresponds to the switch from the excitable to the oscillatory instability at the initial interface.

The main results predicted from the numerical analysis are qualitatively confirmed by means of experiments performed with the ferroin-catalyzed BZ system in a two-dimensional geometry. Two gels were loaded each with part of the BZ reactants and put in contact along a flat line to obtain an initial condition equivalent to the one imposed in the [Numerical Study](#). Once the gels were in contact, reaction–diffusion fronts and waves developed. Indeed, an autocatalytic front was observed across side α while waves emanated from the oxidized zone and propagated toward side β . At high concentrations of malonic acid, additional waves nucleated at the center of the reactor. The effect of varying the concentration of malonic acid on the characteristics of the waves is qualitatively similar to the trends obtained numerically.

Our theoretical approach has been validated as a robust means of describing interfacial pattern formation in two-layer systems with the BZ reaction. Nevertheless, this study represents just a first step toward extending the theory of the classic $A + B \rightarrow C$ problem to a new class of systems in which interfacial autocatalytic and oscillatory kinetics take place. We have shown, for instance, that in the presence of an autocatalytic reaction a diffusion-limited autocatalytic front can start at the initial interface and develops toward both sides of the reactor. Different from the $A + B \rightarrow C$ case, the $A + B \rightarrow$ oscillator front grows symmetrically or asymmetrically around the contact line only depending on whether the reactants have the same diffusivity or not, respectively, while the dynamics is independent from the concentration ratio between the two initial reactants. Also, unlike the dynamics in a medium where the initial reactants are initially homogeneously distributed, diffusion-limited autocatalytic fronts do not develop with a constant velocity; instead, their speed depends on the local concentration of the reactants. This property, which explains the anisotropic growth of the front when differential diffusion is at play, was quantitatively described (see [eq 8](#)).

An even richer variety of RD dynamics can be expected with $A + B \rightarrow$ oscillator systems as different kinds of instability separated in space could interact, such as traveling waves and stationary structures. In the future, new experimental and theoretical investigations in this context are envisaged.

To conclude, this study paves the way for building up a reference framework of interfacial dynamics driven by reaction–diffusion-limited processes which is fundamental for interpreting more complex phenomena encountered in the realm of RDC systems.

■ ASSOCIATED CONTENT

📄 Supporting Information

The Supporting Information is available free of charge on the ACS Publications website at DOI: [10.1021/acs.jpca.5b10802](https://doi.org/10.1021/acs.jpca.5b10802).

Derivation of the kinetic equations and description of related parameters used in numerical simulations ([PDF](#)).

■ AUTHOR INFORMATION

Corresponding Author

*E-mail: mabudroni@uniss.it.

Author Contributions

§M.A.B. and L.L. contributed equally to this work.

Notes

The authors declare no competing financial interest.

■ ACKNOWLEDGMENTS

M.A.B. gratefully acknowledges Regione Sardegna for financial support in the framework of “Asse IV Capitale Umano, Obiettivo Operativo I.3 Linea di Attività I.3.1 del P.O.R. Sardegna F.S.E. 2007/2013 - Progetti in forma associata e/o partenariale C.U.P. E85E12000060009”. A.D. and L.L. acknowledge funding by FRIA, PRODEX, and Fonds Van Buuren. A.P.-M. and D.E. acknowledge financial support by Xunta de Galicia under Project GPC2015/014.

■ REFERENCES

- (1) Gálfi, L.; Rácz, Z. Properties of the reaction front in an $A + B \rightarrow C$ type reaction-diffusion process. *Phys. Rev. A: At, Mol., Opt. Phys.* **1988**, *38*, 3151–3154.
- (2) Jiang, Z.; Ebner, C. Simulation study of reaction fronts. *Phys. Rev. A: At, Mol., Opt. Phys.* **1990**, *42*, 7483–7486.
- (3) Koza, Z. The long-time behavior of initially separated $A + B \rightarrow 0$ reaction-diffusion systems with arbitrary diffusion constants. *J. Stat. Phys.* **1996**, *85*, 179–191.
- (4) Koo, Y. E.; Li, L.; Kopelman, R. Reaction front dynamics in diffusion-controlled particle-antiparticle annihilation: experiments and simulations. *Mol. Cryst. Liq. Cryst. Inc. Nonlinear Opt.* **1990**, *183*, 187–192.
- (5) Taitelbaum, H.; Koo, Y.-E. L.; Havlin, S.; Kopelman, R.; Weiss, G. H. Exotic behavior of the reaction front in the $A + B \rightarrow C$ reaction-diffusion system. *Phys. Rev. A: At, Mol., Opt. Phys.* **1992**, *46*, 2151–2154.
- (6) Yen, A.; Koo, Y.-E. L.; Kopelman, R. Experimental study of a crossover from nonclassical to classical chemical kinetics: An elementary and reversible $A + B \rightleftharpoons C$ reaction-diffusion process in a capillary. *Phys. Rev. E: Stat. Phys., Plasmas, Fluids, Relat. Interdiscip. Top.* **1996**, *54*, 2447–2450.
- (7) Liesegang, R. E. Ueber einige eigenschaften von gallerten. *Naturwiss. Wochenschr.* **1896**, *11*, 353–362.
- (8) Grzybowski, B. A. *Chemistry in motion: Reaction-diffusion systems for micro- and nanotechnology*; Wiley: Chichester, UK, 2009.

- (9) Haudin, F.; Cartwright, J. H. E.; Brau, F.; De Wit, A. Spiral precipitation patterns in confined chemical gardens. *Proc. Natl. Acad. Sci. U. S. A.* **2014**, *111*, 17363–17367.
- (10) Makki, R.; Roszol, L.; Pagano, J. J.; Steinbock, O. Tubular precipitation structures: materials synthesis under non-equilibrium conditions. *Philos. Trans. R. Soc., A* **2012**, *370*, 2848–2865.
- (11) Glaab, F.; Kellermeier, M.; Kunz, W.; Morallon, E.; García-Ruiz, J. M. Formation and evolution of chemical gradients and potential differences across self-assembling inorganic membranes. *Angew. Chem., Int. Ed.* **2012**, *51*, 4317–4321.
- (12) Rongy, L.; Trevelyan, P. M. J.; De Wit, A. Dynamics of $A + B \rightarrow C$ reaction fronts in the presence of buoyancy-driven convection. *Phys. Rev. Lett.* **2008**, *101*, 084503.
- (13) Almarcha, C.; Trevelyan, P. M. J.; Grosfils, P.; De Wit, A. Chemically driven hydrodynamic instabilities. *Phys. Rev. Lett.* **2010**, *104*, 044501.
- (14) Nagatsu, Y.; Ishii, Y.; Tada, Y.; De Wit, A. Hydrodynamic fingering instability induced by a precipitation reaction. *Phys. Rev. Lett.* **2014**, *113*, 024502.
- (15) Sherwood, T.; Wei, J. Interfacial phenomena in liquid extraction. *Ind. Eng. Chem.* **1957**, *49*, 1030–1034.
- (16) Avnir, D.; Kagan, M. Spatial structures generated by chemical reactions at interfaces. *Nature* **1984**, *307*, 717–720.
- (17) Hassanzadeh, H.; Pooladi-Darvish, M.; Keith, D. W. Accelerating CO_2 dissolution in saline aquifers for geological storage - mechanistic and sensitivity studies. *Energy Fuels* **2009**, *23*, 3328–3336.
- (18) Loodts, V.; Thomas, C.; Rongy, L.; De Wit, A. Control of convective dissolution by chemical reactions: general classification and application to CO_2 dissolution in reactive aqueous solutions. *Phys. Rev. Lett.* **2014**, *113*, 114501.
- (19) Lemaigre, L.; Budroni, M. A.; Riolfo, L. A.; Grosfils, P.; De Wit, A. Asymmetric Rayleigh-Taylor and double-diffusive fingers in reactive systems. *Phys. Fluids* **2013**, *25*, 014103.
- (20) Kapral, R.; Showalter, K. *Chemical waves and patterns*; Kluwer: Dordrecht, The Netherlands, 1995.
- (21) Epstein, I. R.; Pojman, J. A. *An introduction to nonlinear chemical dynamics*; Oxford University Press: Oxford, UK, 1998.
- (22) Gray, P.; Scott, S. K. *Chemical oscillations and instabilities. Non-linear chemical kinetics*; Oxford University Press: Oxford, UK, 1994.
- (23) Zaikin, A. N.; Zhabotinsky, A. M. Concentration wave propagation in two-dimensional liquid-phase self-oscillating system. *Nature* **1970**, *225*, 535–537.
- (24) Vanag, V. K.; Epstein, I. R. Pattern formation in a tunable medium: The Belousov-Zhabotinsky reaction in an aerosol OT microemulsion. *Phys. Rev. Lett.* **2001**, *87*, 228301.
- (25) Pojman, J. A.; Epstein, I. R. Convective effects on chemical waves. I. Mechanisms and stability criteria. *J. Phys. Chem.* **1990**, *94*, 4966–4972.
- (26) Wu, Y.; Vasquez, D. A.; Edwards, B. F.; Wilder, J. W. Convective chemical-wave propagation in the Belousov-Zhabotinsky reaction. *Phys. Rev. E: Stat. Phys., Plasmas, Fluids, Relat. Interdiscip. Top.* **1995**, *51*, 1119–1127.
- (27) Rongy, L.; Schusztzer, G.; Sinkó, Z.; Tóth, T.; Horváth, D.; Tóth, A.; De Wit, A. Influence of thermal effects on buoyancy-driven convection around autocatalytic chemical fronts propagating horizontally. *Chaos* **2009**, *19*, 023110.
- (28) Horváth, D.; Budroni, M. A.; Baba, P.; Rongy, L.; De Wit, A.; Eckert, K.; Hauser, M. J. B.; Tóth, A. Convective dynamics of traveling autocatalytic fronts in a modulated gravity field. *Phys. Chem. Chem. Phys.* **2014**, *16*, 26279–26287.
- (29) Rongy, L.; De Wit, A.; Homsy, G. M. Asymptotic structure of steady nonlinear reaction-diffusion-Marangoni convection fronts. *Phys. Fluids* **2008**, *20*, 072103.
- (30) Rossi, F.; Budroni, M. A.; Marchettini, N.; Carballido-Landeira, J. Segmented waves in a reaction-diffusion-convection system. *Chaos* **2012**, *22*, 037109.
- (31) Budroni, M. A.; Rongy, L.; De Wit, A. Dynamics due to combined buoyancy- and Marangoni-driven convective flows around autocatalytic fronts. *Phys. Chem. Chem. Phys.* **2012**, *14*, 14619–14629.
- (32) De Wit, A.; Eckert, K.; Kalliadasis, S. Introduction to the focus issue: chemo-hydrodynamic patterns and instabilities. *Chaos* **2012**, *22*, 037101.
- (33) Pérez-Villar, V.; Muñuzuri, A. P.; Lorenzo, M. N.; Muñuzuri, V. P. Spiral wave meandering induced by fluid convection in an excitable medium. *Phys. Rev. E: Stat. Phys., Plasmas, Fluids, Relat. Interdiscip. Top.* **2002**, *66*, 036309.
- (34) Marchettini, N.; Budroni, M. A.; Rossi, F.; Masia, M.; Turco Liveri, M. L.; Rustici, M. Role of the reagents consumption in the chaotic dynamics of the Belousov-Zhabotinsky oscillator in closed unstirred reactors. *Phys. Chem. Chem. Phys.* **2010**, *12*, 11062–11069.
- (35) Budroni, M. A.; Rustici, M.; Tiezzi, E. On the origin of chaos in the Belousov-Zhabotinsky reaction in closed and unstirred reactors. *Math. Modell. Nat. Phenom.* **2011**, *6*, 226–242.
- (36) Ciotti, L.; Budroni, M. A.; Masia, M.; Marchettini, N.; Rustici, M. Competition between transport phenomena in a reaction-diffusion-convection system. *Chem. Phys. Lett.* **2011**, *512*, 290–296.
- (37) Escala, D. M.; Budroni, M. A.; Carballido-Landeira, J.; De Wit, A.; Muñuzuri, A. P. Self-organized traveling chemo-hydrodynamic fingers triggered by a chemical oscillator. *J. Phys. Chem. Lett.* **2014**, *5*, 413–418.
- (38) Nicolis, G.; Prigogine, I. *Self-Organization in nonequilibrium systems*; Wiley: New York, 1977.
- (39) Boissonade, J. Stationary structure induced along a reaction-diffusion front by a Turing symmetry breaking instability. *J. Phys. (Paris)* **1988**, *49*, 541–546.
- (40) Castets, V.; Dulos, E.; Boissonade, J.; De Kepper, P. Experimental evidence of a sustained standing Turing-type nonequilibrium chemical pattern. *Phys. Rev. Lett.* **1990**, *64*, 2953–2956.
- (41) Lengyel, I.; Rabai, G.; Epstein, I. R. Experimental and modeling study of oscillations in the chlorine dioxide-iodine-malonic acid reaction. *J. Am. Chem. Soc.* **1990**, *112*, 9104–9110.
- (42) Borckmans, P.; De Wit, A.; Dewel, G. Competition in ramped Turing structures. *Phys. A* **1992**, *188*, 137–157.
- (43) Dewel, G.; Borckmans, P.; De Wit, A.; Rudovics, B.; Perraud, J.-J.; Dulos, E.; Boissonade, J.; De Kepper, P. Pattern selection and localized structures in reaction-diffusion systems. *Phys. A* **1995**, *213*, 181–198.
- (44) Belousov, B. P. A periodic reaction and its mechanism. *Sbornik Referatov po Radiatsionno Meditsine. Moscow* **1958**, 145–147.
- (45) Noszticzus, Z.; Horsthemke, W.; McCormick, W.; Swinney, H.; Tam, W. Sustained chemical waves in an annular gel reactor: a chemical pinwheel. *Nature* **1987**, *329*, 619–620.
- (46) Dulos, E.; Boissonade, J.; De Kepper, P. Dynamics and morphology of sustained two-dimensional wavetrains. *Phys. A* **1992**, *188*, 120–131.
- (47) Budroni, M. A.; Rossi, F. A novel mechanism for in situ nucleation of spirals controlled by the interplay between phase fronts and reaction-diffusion waves in an oscillatory medium. *J. Phys. Chem. C* **2015**, *119*, 9411–9417.
- (48) Amemiya, T.; Kádár, S.; Kettunen, P.; Showalter, K. Spiral wave formation in three-dimensional excitable media. *Phys. Rev. Lett.* **1996**, *77*, 3244–3247.
- (49) Field, R. J.; Korös, E.; Noyes, R. M. Oscillations in chemical systems. II. Thorough analysis of temporal oscillation in the bromate-cerium-malonic acid system. *J. Am. Chem. Soc.* **1972**, *94*, 8649–8664.
- (50) Manz, N.; Hamik, C. T.; Steinbock, O. Tracking waves and vortex nucleation in excitable systems with anomalous dispersion. *Phys. Rev. Lett.* **2004**, *92*, 248301.